ROYAL SOCIETY OPEN SCIENCE

rsos.royalsocietypublishing.org

Research

Article submitted to journal

Subject Areas:
foodwebs, paleontology, ecology

Keywords:
foodwebs, mammals, foraging

Author for correspondence:
Taran Rallings
e-mail: trallings@ucmerced.edu

On the dynamics of starvation, mortality, and the ephemeral nature of mammalian megafauna

Taran Rallings[1], Christopher P Kempes[2], Justin D. Yeakel[1]

[1]School of Natural Sciences, University of California Merced
[2]Santa Fe Institute

The vital rates constraining energy flow through consumer-resource interactions largely vary as a function of body size. These allometric relationships govern the dynamics of populations, and the energetic constraints induced by different sources of mortality have influence small- to large-bodied species in different ways. Here we derive the timescales associated with four alternative sources of mortality for terrestrial mammals: starvation from resource limitation, mortality associated with aging, consumption by specialist to generalist predators, and that introduced by subsidized harvest. The incorporation of these allometric relationships into a minimal consumer-resource dynamic system illuminates central constraints that may contribute to the structure of mammalian communities. Our framework reveals that while starvation largely impacts smaller-bodied species, the allometry of senescence is expected to be more difficult to observe. In contrast, external predation and subsidized harvest primarily influence larger-bodied species. The inclusion of predation mortality reveals mass thresholds of mammalian herbivores, where dynamic instabilities limit the feasibility of megaherbivore populations. Moreover, we show how these thresholds vary with predator-prey mass ratios, a relationship that is little understood within terrestrial systems. Finally, we predict the harvest pressure required to induce mass-specific extinction, and compare these values to estimates from episodes of both paleontological and historical megafaunal exploitation.

THE ROYAL SOCIETY PUBLISHING

1. Introduction

Consumer-resource interactions are the fundamental unit from which complex food webs arise [1], where the rates governing transitions of biomass and energy from one species to another are largely determined by their respective body sizes [2]. The allometric relationships between consumer body mass and metabolism constrain energetic assimilation [3], storage [4], and growth [5], and therefore govern the dynamics of populations [6–9]. Because allometrically-constrained models of population dynamics apply generally across large taxonomic clades, they are useful for examining dynamic constraints that may contribute to community structure across macroevolutionary timescales [9,10]. Furthermore, examination of community dynamics at these scales enables the investigation of extinct communities where body size distributions were different than those in contemporary ecosystems [11–13].

The dynamics of populations represent an energetic balance between reproduction and mortality [14]. While reproduction is unique with predictable allometric scaling relationships [15], mortality has a variety of forms that do not all scale similarly. Mortality originates from internal or external drivers, where the former depends on an organism's internal state to initiate death. For example, senescence and starvation involve physiological states that change with respect to time and resource depletion, respectively [9,16]. In contrast, external drivers of mortality consist of an outside force that induces death regardless of an organism's internal state, such as mortality due to natural predation or subsidized anthropogenic harvest. Often mortality occurs through correlations between internal and external drivers, where for example, starvation experienced by prey may alter rates of predation [17]. While virtually all primary consumer populations must deal with the effects of resource limitation, aging, and predation, the effects of harvesting are uniquely limited to those species serving as resources for subsidized human populations [18].

How do different sources of mortality impact the dynamics of mammalian populations? Here we construct a general consumer-resource framework to examine mammalian herbivore populations as a function of consumer body size M_C, as well as size-dependent vulnerability to different internal and external pressures. Because our approach integrates relationships governing specific physiological and assimilational timescales from a process-based energetic perspective [5], it is both low-dimensional [cf. 9] and capable of reproducing large-scale empirical patterns of mammalian communities. We begin by describing our approach, reproducing key macroecological relationships such as Damuth's law [19], and examining how changes to energetic parameters impact predictions. We then derive timescales associated with four sources of mortality experienced by mammalian consumers: *i*) natural mortality, *ii*) starvation mortality, *iii*) natural predation, and *iv*) subsidized anthropogenic harvesting. By examining each source of mortality in turn, our framework illuminates central constraints governing mass-specific behaviors, strategies, and risks experienced by mammalian consumers.

Our results reveal four key insights into the constraints structuring mammalian communities. First, our allometric consumer-resource system accurately captures both the central tendency and variability of Damuth's law, suggesting that the included vital rates accurately capture mass-specific dynamics. Second, our results demonstrate that natural and starvation mortality differentially impact small mammals, confirming expectations, and point to why the allometric effects of senescence are difficult to observe in nature. Third, we detail how mortality from specialist or generalist predators induce population instabilities for large-bodied herbivores, and that the body size at which these instabilities occur are dependent on the prevailing predator-prey mass ratios (PPMRs). Finally, we evaluate the harvest pressure required to induce mass-specific extinction, and show that our predictions are comparable to estimates of both paleontological and historical exploitation of mammalian megafauna.

2. Allometric Consumer-Resource Model

We model a consumer-resource interaction, where the resource R (g/m^2) grows logistically with intrinsic growth rate α to a carrying capacity k, and declines due to consumption by an herbivore consumer population C (g/m^2) (Eq. 2.2). Consumed resources govern both consumer somatic maintenance and reproduction. The rate of consumption to fuel somatic maintenance is given by ρ, and is independent of resource density, as these are invariant requirements of the consumer population [9]. In contrast, the rate of consumption to fuel reproduction is proportional to resource density and is given by $\lambda_C(R)/Y_C$, where $\lambda_C(R)$ is the consumer growth rate and Y_C is the consumer yield coefficient, or the grams of consumer produced per gram of resource consumed (see Supplementary Materials Appendix XX). As in DeLong & Vasseur [20], the consumer's growth rate $\lambda_C(R)$ follows Michaelis-Menton (Type II) kinetics as a function of the resource density R, where the maximum growth is λ_C^{max} and the resource half-saturation density is $\hat{k} = k/2$, such that

$$\lambda_C(R) = \lambda_C^{max}\left(\frac{R}{\hat{k}+R}\right). \tag{2.1}$$

While the consumer population density grows at rate $\lambda_C(R)$, we assume for now that consumer mortality is a function of both natural mortality μ and starvation, where the rate of starvation $\sigma(1-R/k)$ increases as resources become scarce. In this context, σ is the maximal rate of starvation that occurs when the environment is devoid of resources. The full system describing resource and consumer dynamics is given by

$$\begin{aligned}\frac{d}{dt}C &= \lambda_C(R)C - \left(\mu + \sigma\left(1-\frac{R}{k}\right) + ...\right)C,\\ \frac{d}{dt}R &= \alpha R\left(1-\frac{R}{k}\right) - \left(\frac{\lambda_C(R)}{Y_C} + \rho\right)C,\end{aligned} \tag{2.2}$$

where the '...' denotes where additional mortality terms, described later, will be included. The dynamic outcomes of this system of equations include two trivial steady states at $(R^* = 0, C^* = 0)$ and $(R^* = k, C^* = 0)$, and one internal steady state where both the consumer and resource population coexist. Because the internal steady state cannot be concisely written, we do not report it here. See Table 1 for a description of parameters.

The rate laws describing resource consumption as well as consumer growth and mortality all vary as a function of consumer body mass M_C, where the consumer is assumed to be a mammalian herbivore, and the resource is an unspecified plant functional group with characteristic growth rate α, carrying capacity k, and energy density E_d. We approach the derivation of vital rates with respect to consumer mass by solving for multiple timescales associated with ontogenetic growth, maintenance, and expenditure. The growth of an individual consumer from birth mass $m = m_0$ to its reproductive size $m = 0.95M_C$ is given by the solution to the general balance condition $B_0 m^\eta = E_m \dot{m} + B_m m$, where E_m is the energy needed to synthesize a unit of biomass, B_m is the metabolic rate to support an existing unit of biomass, and the metabolic exponent $\eta = 3/4$ [5]. From this balance condition, the time required for an organism starting from mass m_1 to reach mass m_2 follows

$$\tau(m_1, m_2) = \ln\left(\frac{1-(m_1/M_C)^{1-\eta}}{1-(m_2/M_C)^{1-\eta}}\right)\frac{M_C^{1-\eta}}{a(1-\eta)} \tag{2.3}$$

where $a = B_0/E_m$. From this general equation, we calculate the timescale of reproduction for an herbivore consumer of mass M_C as $t_\lambda = \tau(m_0, 0.95M_C)$, such that the reproductive rate is $\lambda_C^{max} = \ln(\nu)/t_\lambda$, where $\nu = 2$ is the set number of offspring per reproductive cycle [9,21]. The consumer yield coefficient $Y_C = M_C E_d / B_\lambda$ (g consumer per g resource) where B_λ is the lifetime energy use required to reach maturity $B_\lambda = \int_0^{t_\lambda} B_0 m(t)^\eta dt$ [9]. The maintenance rate is given by $\rho = B_0 M_C^\eta / M_C E_d$.

To determine the rate of mortality from starvation, we calculate the time required for an organism to metabolize its endogenous energetic stores, estimated from its cumulative fat and

muscle mass, where the remaining mass is given by $M_C^{\text{starve}} = M_C - (M_C^{\text{fat}} + M_C^{\text{musc}})$ (see Table xx). During starvation, we assume that an organism burns its existing endogenous stores as its sole energy source, where the balance condition is altered to $\dot{m}E'_m = -B_m m$, where E'_m is the amount of energy stored in a unit of biomass (differing from the amount of energy used to synthesize a unit of biomass E_m). The starvation timescale is then given by

$$t_\sigma = -\frac{M_C^{1-\eta}}{a'} \ln(M_C^{\text{starve}}/M_C), \tag{2.4}$$

where $a' = B_0/E'_m$, such that the starvation rate is the $\sigma = 1/t_\sigma$.

To determine the rate of mortality from aging, we note that population cohorts experience two primary sources of natural mortality: the initial cohort mortality rate q_0 and the annual rate of increase in mortality as the cohort ages, or the actuarial aging rate, q_a over lifetime t_ℓ. We begin by assuming that the number of survivors over time follows a Gompertz relationship [9,15] from which we can derive the average rate of natural mortality

$$\mu = \frac{q_0}{q_a t_\ell}\big(\exp(q_a t_\ell) - 1\big). \tag{2.5}$$

The three parameters (q_0, q_a, t_ℓ) each have well-documented allometric relationships for terrestrial mammals, such that natural mortality can be written as a function of consumer mass $\mu(M_C)$ (see Supplementary Materials Appendix XX).

We emphasize that while the sizes of physiological biomass compartments are obtained from empirically-measured relationships, the rates determining biomass flux are derived from process-based energetic relationships. Together, the allometric rate laws and the dynamic system presented in Eq. 2.2 allow us to assess the dynamics of consumer-resource systems for mammalian herbivores spanning the observed range of terrestrial body sizes, from the smallest (the Etruscan shrew at ca. 1 g) to the largest (the Oligocene paraceratheres and Miocene deinotheres at ca. $1.5 - 1.74 \times 10^7$ g) [22]. We next examine how this minimal framework is well-suited to provide general insight into several key allometric constraints that contribute to the functioning and limitations of terrestrial mammalian communities.

3. Results and Discussion

(a) Recovering Damuth's mass-density relationship

Our consumer-resource system is related to the 3-dimensional nutritional state model (NSM) proposed in Yeakel et al. [9], where an explicit starvation dynamic was incorporated by separating the consumer population density into a 'full' and 'hungry' state. Because the timescales of transitioning between full and hungry states are short relative to those of reproduction, we sacrifice a modest degree of physiological realism to enable analytical expression of steady states with additional sources of mortality. After substituting allometric relationships into the rate laws in Eq. 2.2, we observe that the internal steady state of the consumer is very close to observations of mammalian densities in natural systems, thereby approximating Damuth's Law (blue line in Fig. 1). Compared to the NSM [9], and similar to DeLong & Vasseur [23], we observe slightly exaggerated densities for small-bodied consumers, though within the observed range of variation. This overestimate is not observed when explicit starvation and recovery are included [9], suggesting these dynamics play an important role in depressing the populations of smaller-bodied species. The allometric consumer-resource model provides an approximation to the mass-density relationship observed among terrestrial herbivorous mammals [19]. Incorporating observed variations in measured values for α and k reveals strong alignment between model predictions and the observed variability of densities across mammalian clades (Fig. 1). We examine the effects of variation for other vital rates in Supplementary Materials Appendix XX.

(b) Natural mortality and starvation impact smaller consumers

We first consider two internal sources of mortality: that due to the effects of aging, where mortality scales with an organism's temporal state, and that due to starvation, where mortality scales with an organism's energetic state. Immediate insight into system constraints can be gained by examining how the rates of consumer mortality compare to reproduction, with the expectation that stability requires mortality rates to be lower than reproductive rates (Fig. 2A). The starvation rate is a key exception: because organisms can starve and recover many times over the course of their lifetime, the maximal rate of starvation $\sigma(M_C) > \lambda_C(M_C)$, whereas the realized starvation rate is lower. We observe that natural mortality, including both initial cohort mortality and actuarial mortality, is much lower and projects a steeper slope over M_C than the rates of reproduction and starvation-induced mortality (Fig. 2B), with a scaling $\propto M_C^{-0.56}$ [cf. 24]. While the calculated value of μ is nearly one order of magnitude below the rate of reproduction λ_C, a steeper slope implies that increases in μ will disproportionately harm smaller organisms.

To understand the effect of changes to $\mu(M_C)$ on consumer steady states, we examine variations in the principle components of μ: initial cohort mortality q_0 and actuarial mortality q_a. The initial cohort mortality represents the mortality experienced by a cohort prior to the accruing effects of age. As q_0 is altered, we observe the mortality rate to change in direct proportion, independent of consumer mass. For survivorship mortality to approach the rate of reproduction, where perceptible declines in population densities result, the initial cohort mortality must increase by roughly an order of magnitude (shaded region in Fig. 2A), and due to the steepness of μ, this effect is felt exclusively by small-bodied organisms (Fig. 2B).

Actuarial mortality represents the cumulative effects of aging, or senescence, across the organism's expected lifetime. We observe that as q_a increases, the magnitude of mortality rises while the slope of $\mu(M_C)$ becomes more shallow (Fig. 2C), primarily due to the cumulative nature of senescence magnifying its effects across the longer lifetimes of larger mammals. As such, an order of magnitude increase overwhelms the reproduction of mammals up to ca. 1.2×10^3 g (Fig. 2D), resulting in population instability. The extinction risk imposed by senescence has been explored across mammalian taxa, and while some life history characteristics such as the inter-birth interval appear to correlate strongly with these risks, the role of body size is notably ambiguous [16]. Though our model – which considers averaged effects across terrestrial mammals – predicts that the most extreme risks imposed by increased actuarial mortality impacts smaller size-classes, we also show that μ increasingly resembles λ_C with increasing q_a (the top border of the shaded region in Fig. 2C). This increased similarity implies that relatively small variations in other demographic processes or interactions may have potentially large and destabilizing effects on population size that cannot be predicted from body size, a potential source for the noted ambiguity of allometry and actuarial extinction risk [16].

While the temporal state of an organism is unidirectional and linear, other internal states, such as an organism's energetic state, fluctuate nonlinearly over time. In this case, the rate of starvation is low when resources become plentiful ($R \to k$) and increases to the maximum σ as resources become scarce ($R \to 0$). Because organisms metabolize their fat and muscle tissue during starvation, and die from starvation when these energetic stores are fully metabolized, the timescale of starvation varies with the amount of endogenous energetic stores an organism carries. Larger organisms carry a larger proportion of body mass as fat [4], such that they are more protected from the effects of short-term resource limitation [25]. We observe this effect by modifying the starvation rate and examining how the steady state population size is altered. We introduce variation to the rate of starvation as $\sigma(1 + \chi_s)$, such that the relative change in the steady state ΔC_s^* introduced by the modified rate is calculated as

$$\Delta C_s^* = \frac{C^*(M_C|\sigma(1+\chi_s)) - C^*(M_C|\sigma)}{C^*(M_C|\sigma)}, \tag{3.1}$$

where higher values indicate a relative gain in steady state densities from the proportional change χ_s, and negative values indicate a relative loss (Fig. 3). We observe that, while all mammals benefit

from reduced starvation rates ($\chi_s < 0$), smaller-bodied mammals benefit to a much greater extent, and this effect tapers off with increasing body mass. Because fat biomass scales super-linearly with body mass, the populations of larger consumers are more resilient to the effects of starvation, whereas those of smaller consumers are more prone.

An organism's rate of starvation emerges from two governing forces – the amount of energy storage and the rate of its use – and as such can be be manipulated both physiologically and behaviorally. For instance, behaviorally supplementing endogenous fat stores with exogenous caches magnifies an individual's energetic stores [26], whereas physiologically-mediated responses to starvation risk such as torpor can introduce significant temporal delays to the effects of resource scarcity [27]. In both cases the time required to pass from a replenished to a starved state is effectively increased, lowering the rate of starvation. The predicted benefits of such adaptations to mammalian steady state densities will be realized primarily by smaller mammals (Fig. 3, Supplementary Appendix Fig. XX), and it is these size classes where traits such as caching and torpor are most common [26,28,29].

(c) Predation mortality and the feasibility of megatrophic interactions

Predators introduce an external source of mortality on prey populations, fueling their own population growth in whole (trophic specialists) or in part (trophic generalists), by the rate at which prey are consumed. We account for the effects of an implicit predator density P with body size M_P on the herbivore consumer density C with body size M_C. The mortality rate of the herbivore consumer from an external predator is given by

$$\beta(C,P) = f\frac{\lambda_P(C)P}{CY_P}, \tag{3.2}$$

where $\lambda_P(C)$ is the growth rate of the predator and Y_P is the predator yield coefficient, describing the grams of predator produced per gram of prey consumed (see Supplementary Materials Appendix XX), and f is the degree of specialization of the predator on the consumer prey ($f = 1$ denotes specialization, whereas $f < 1$ denotes generalization). Assuming a linear functional response for predation mortality, $\lambda_P(C)$ is maximized when the consumer reaches its theoretical maximum population density, which we calculate by converting the resource carrying capacity directly to grams of consumer produced, or $C^{\max} = Y_C k$. While this is an ultimately unattainable theoretical bound, it allows for a direct calculation of the predator growth rate as a function of C, written as

$$\lambda_P(C) = \lambda_P^{\max}\frac{C}{C^{\max}} = \lambda_P^{\max}\frac{C}{Y_C k}, \tag{3.3}$$

where $\lambda_P^{\max}$ is the maximum predator growth rate. The theoretical boundary density for herbivore consumers $C^{\max}$ can similarly be used to calculate the boundary density for predators, $P^{\max} = Y_P C^{\max}$, both of which accurately capture the upper-bounds of herbivore and carnivore mass-density relationships (dashed lines in Fig. 4A). Because the effects of the predator are implicit, we assume that the predator population remains at empirically measured steady state densities for mammalian carnivores, where $P \equiv P^* = P_0 M_P^{-0.88}$ (Table 1) [30].

The predation mortality rate depends on both the body size of the herbivore consumer and its respective predator. Trophic interactions are constrained by body size [31–33], and large prey generally suffer mortality from large predators, though the nature of predator-prey mass ratios (PPMRs) varies across communities [34], organismal body size [32,35–38], and is not well understood outside of aquatic gape-limited systems [39]. Because our framework is prey-centric, we require a prediction of the expected predator mass given an herbivore of body size M_C, which cannot be directly extrapolated from the expected prey mass for a given predator mass (see Supplementary Appendix XX). For larger predators and prey ($> 10^5$ g) [40–42], the expected predator mass given a particular herbivore consumer mass follows roughly $\mathrm{E}(M_P|M_C) = p_0 M_C^{p_1}$, where $p_0 = 1.18 \times 10^4$ g and $p_1 = 0.19$ (see Supplementary Appendix XX). Accordingly, larger terrestrial herbivores tend to suffer mortality from proportionately smaller predators,

an asymmetry that becomes more pronounced with increasing size [cf. 31]. We note that smaller terrestrial predator/prey size classes tend to follow different PPMR relationships, where predators tend to be much larger than prey (e.g. rodent- or insect-specialist mesocarnivores) [43,44].

Integrating the large-bodied PPMR relationship into the predation mortality rate reveals the emergence of a dynamic instability at megaherbivore size classes (Fig. 4A), where here and throughout the prefix 'mega' is used to signify size classes $> 6 \times 10^5$ g [40]. An implicit predator population with body size $\mathrm{E}(M_P|M_C)$ is thus able to withdraw sufficient biomass from an herbivore prey population to sustain itself, without crashing the herbivore population, below a threshold herbivore size of $M_C^\dagger = 2.58 \times 10^6$ g (Fig. 4A). Above this critical size threshold, the herbivore population has such low densities that it is unable to sustain a specialist predator species large enough to consume it, introducing a strong upper-bound to mammalian carnivore body size driven by a trophic cascade. This boundary matches the herbivore maximum size limit observed in contemporary terrestrial systems, at roughly the size of an elephant [31] (Fig. 4B; Supplementary Fig. XX).

While $M_C^\dagger$ marks the threshold herbivore mass above which predation is unsustainable, Sinclair et al. [31] have shown contemporary herbivores to begin to escape predation at ca. 4.22×10^5 g (redrawn in Fig. 4B). This change-point reflects the limitations of contemporary carnivores, which reach a maximum body size of 1.15 to 2.60×10^5 g [31,40], and have preferences for prey up to 5.50×10^5 g [40]. As such, the sole predators of contemporary giants are not megaherbivore specialists, instead opportunistically subsidizing their preferred prey base. While we have so far assumed a specialized predator-prey interaction, the largest predators in natural systems tend be dietary generalists [31]. We observe that increasing the implicit dietary generality of the predator (such that $f < 1$) increases $M_C^\dagger$ to a larger threshold mass. For example, $f = 0.37$ means that a predator is supporting a little more than $1/3$ of its growth rate by the targeted prey, increasing the herbivore body mass boundary to $M_C^\dagger = 1.75 \times 10^7$ grams (Fig. 4B; Supplementary Figs. **??**,**??**), roughly the body mass attained by the largest terrestrial herbivores, the Oligocene paraceratheres and Miocene deinotheres [9,22]. That the threshold herbivore mass decreases with increasing predator specialization both suggests that larger predators are dynamically constrained to be dietary generalists [31], while also pointing to an amplifying feedback mechanism [12] that may operate in diverse communities undergoing megafaunal extinctions. As megaherbivore species are lost, the largest predators must respond by increasing their reliance on those remaining. Our results reveal that this energetic redirection will reduce the threshold herbivore mass $M_C^\dagger$ to lower size classes, thereby promoting additional extinctions and attendant predator specialization.

While deinotheres and paraceratheres top the megaherbivore scale, the Eocene artiodactyl *Andrewsarchus* may have been the largest terrestrial mammalian predator of up to 1×10^6 g [45], while the Miocene Hyaenodontid *Megistotherium osteothlastes* ranged between 5 to 8×10^5 g and the early Eocene Oxyaenodont *Sarkastodon mongoliensis* weighed ca. 8×10^5 g [46] . A theoretical maximum mammalian carnivore size of 1.1×10^6 g has been proposed based on the intersection of daily energetic uptake requirements against metabolic expenditures [47], closely aligning with the largest known megapredators. While our consumer-resource framework provides a range of predicted megaherbivore body mass thresholds depending on the fraction of predator growth it fuels, we next ask under what conditions megatrophic relationships between megaherbivores and megapredators are dynamically feasible.

A principle relationship in our framework is the allometric PPMR observed for the largest contemporary herbivores and carnivores, however this PPMR cannot account for past megatrophic relationships (Supplementary Appendix XX). While it is unknown whether these super-sized carnivores were specialists on deinothere size-classes (REFS), our framework allows us to investigate whether and to what extent changes to the contemporary PPMR enable megatrophic interactions, where we allow the PPMR to vary as

$$\mathrm{E}(M_P|M_C) = p_0(1 + \chi_{\mathrm{int}})M_C^{p_1(1+\chi_{\mathrm{slope}})}, \tag{3.4}$$

where the proportional changes in the PPMR intercept and slope are given by χ_{int} and $\chi_{\text{slope}} \in (-0.99, 2)$. We find that the threshold herbivore body size $M_C^{\dagger}$ increases, while $M_P^{\dagger}$ decreases, with lower PPMR intercepts and shallower slopes (Fig. 4C,D). Lower PPMR intercepts and shallower slopes mean that predator sizes are generally smaller, and increase more slowly, with larger herbivore body sizes. So given a particular herbivore size, proportionately smaller predators elevate the threshold herbivore mass, while proportionately larger predators drive down the threshold herbivore mass. Importantly, only a small range of values for PPMR intercepts and slopes permit the existence of megatrophic interactions where megaherbivores ($1.72 - 2.01 \times 10^6$ g) serve as prey for megapredators ($6.11 \times 10^5 - 1.19 \times 10^6$ g; white band in Fig. 4C,D). While significantly larger PPMR intercepts ($\chi_{\text{int}} \gg 0$) are unlikely to be realized in natural systems, the megainteraction range does include very low intercepts with very high slopes, such that PPMRs are low at smaller masses, and much higher at large masses. Such an hypothesized PPMR does not stray far from contemporary large-mammal interactions (Supplementary Fig. **??**) and may be a good candidate for megatrophic interactions.

Feasible megatrophic interactions increase substantially if a smaller percentage of the predator growth rate is fueled by the target herbivore population ($f < 1$). Setting $f = 0.37$ – which we observed increases $M_C^{\dagger}$ to deinothere/indricothere size classes – and allowing both χ_{int} and χ_{slope} to vary, results in megatrophic interactions spanning the largest megaherbivore ($1.27 - 1.48 \times 10^7$ g) and megapredator ($6.15 \times 10^5 - 1.20 \times 10^6$ g) sizes observed in the fossil record (Supplementary Fig. **??**). Our framework thus highlights dynamic constraints existing between predators and prey that may serve to structure terrestrial mammalian communities over evolutionary time, in particular revealing the tenuous positions of mega-sized herbivores and predators. As carnivorous clades acquire body sizes enabling megaherbivore predation over evolutionary time, their super-sized appetites may result in unsustainable megaherbivore densities where the risk of extinction becomes overwhelming – an evolutionary trap marking the final tooth in the hypercarnivore ratchet [cf. 48].

(i) Harvesting to extinction

We last consider the effects of anthropogenic harvest-induced mortality on consumer populations. While the predation rate is naturally limited by the energetic needs of the predator, we consider harvest to be a comparatively unconstrained source of mortality. This may be the case if the human population(s) engaged in harvesting are subsidized by alternative resources [49]. Harvest pressure has potentially varying relationships with consumer (prey) body mass, a complex product of environment, climate, culture, and technology [50], where harvest rate $h = \xi M_C^w$. For example, hunting traditions specializing on mass-collecting, by way of trapping or netting [50,51] are expected to exhibit harvest allometries biased towards smaller species (negative size-scaling, $w < 0$), whereas a purely opportunistic strategy may be expected to have very little allometric dependence (zero size-scaling, $w = 0$). Inclusion of negative size-scaling harvest reveals that smaller-sized prey can withstand significant harvesting pressure before their populations are negatively impacted. While smaller mammals do not appear to offer a significant return on investment, the mass-collecting of invertebrates such as grasshoppers, and fish can offer significant returns [51]. In contrast, the inclusion of zero size-scaling harvest reveals that it is the larger-bodied species that are negatively impacted, but only where $h(M_C) > \lambda_C(M_C)$ (Supplementary Fig. **??**).

Technology provides access to otherwise unobtainable size-classes of potential prey, and is expected to strongly influence the allometry of harvesting effort. For example, the innovation of advanced projectiles is thought to have enabled harvest of terrestrial megafauna [50,52], while archeological evidence points to many Pleistocene human populations as potential megafaunal specialists (positive size-scaling, $\ell > 0$) [53]. More recently, historical fisheries have been subject to positive size-scaling harvest efforts [54], and contemporary size classes may be much reduced due to the accumulation of these pressures over time (Jennings 2004) [55]. While the allometry of

harvest effort is largely unknown and highly plastic, our framework allows us to examine how much effort is required to induce population collapse as a function of mammalian body size.

We next calculate the harvest rate required to induce extinction, $h^\dagger$, as a function of body size M_C, and find a scaling relationship proportional to the mass-density relationship where $h^\dagger \propto M_C^{-1/4}$. This is a natural result, as the effort required to suppress a population is expected to be proportional to the consumer's abundance. As a proportion of the other sources of consumer mortality that we have considered (excluding predation; $f = 0$), extinction-level harvesting is lower for smaller consumers, saturating at close to unity for larger consumers, reflecting the elevated role of starvation mortality among small-sized organisms. With predation mortality included from both generalist ($f = 0.37$) and specialist ($f = 1$) predators, extinction-level harvesting accounts for an increasingly smaller proportion of mortality for larger organisms (orange and red lines, Fig. 5A). This highlights the delicate nature of the megafaunal niche, where smaller changes in mortality rates can induce population collapse.

To examine how our estimate of extinction-level harvesting rates $h^\dagger$ compare to those estimated for human hunting of paleontological and historical mammalian populations, we converted $h^\dagger$ to harvest pressure $\psi^\dagger$, or the number of individuals harvested per year to reduce the population to a fraction of its steady state ϵC^* where we set $\epsilon = 0.01$. We calculate $\psi^\dagger$ for an arbitrary area (see Supplementary Appendix XX), which we standardize as the area of California ($A_{\mathrm{CA}} = 4.24 \times 10^5$ km^2), such that

$$\psi^\dagger \propto -h^\dagger \frac{C^*(1-\epsilon)}{M_C \log(\epsilon)}. \tag{3.5}$$

We observe that – though the annual harvesting pressure is unrealistically high for smaller organisms – it is ca. 1.2×10^4 inds/yr/A_{CA} for organisms $> 10^6$ g in the absence of predation mortality ($f = 0$). With the increasing pressures of generalist and specialist predation, the harvest pressure required to induce extinction is much less for these larger consumers (Fig. 5B).

Our predictions of extinction-inducing harvest pressure compare well with paleontological and historical estimates of harvesting pressure on mammalian megafauna. For example, Fordham et al.'s [56] estimate of the harvest pressure required to collapse mammoth (*Mammuthus primigenius*) populations [using a formulation similar to that of Alroy; 11] revealed a range of values consistent with our expectation for similar size-classes (est. harvest pressure = 5.37×10^4 inds/yr/A_{CA}), as did estimates of extinction-inducing harvest of the Australian *Diprotodon* [est. harvest pressure = ca. 763 inds/yr/A_{CA}; 13]. Within the historical record, elephant (*Loxodonta*) populations experienced comparatively lower harvest pressure through 1850 [ca. 466 inds/yr/A_{CA}, derived from the volume of ivory exports; 57]. While fluctuating over the next century, harvest pressure elevated to a maximum of ca. 13.3×10^5 inds/yr/A_{CA} just prior to 1987 (Fig. 5B). This level of harvest was not sustained, as ivory export volume plummeted following the implementation of trade restrictions in 1989 [57]. Both Fordham et al.'s [56] estimate for Pleistocene mammoths and the short-lived harvest maximum for African elephants in 1987 [57] achieved pressures greater than $\psi^\dagger$ under the conservative assumption of zero natural predation. While estimates for *Diprotodon* harvest are considerably lower [13], it is important to note that our measure of harvest pressure is parameterized for eutherian rather than marsupial mammals. Nevertheless, the estimated *Diprotodon* $\psi^\dagger$ is well within range of extinction-inducing harvest rates if natural predation pressures are also included, and there is evidence to suggest that *Diprotodon* likely served as prey for marsupial lions [58,59], and both giant crocodylians (*Pallimnarchus*) and varanid lizards (*Megalania*) [60].

4. Conclusion

We have shown that the inclusion of mass-specific energetic transfer between resources and consumers, combined with the unique timescales governing consumer mortality, both predict Damuth's Law [19] and provide insight into dynamic thresholds constraining populations. While natural and starvation mortality primarily impact small-bodied species, trophic mortality

primarily impacts large-bodied species with longer generational timescales. Moreover, while mass-specific predation gives rise to dynamic thresholds on herbivore populations, these effects are sensitive to both predator generality as well as the associated predator-prey mass ratio, which isn't well understood for terrestrial megafauna [39]. While assessment of particular communities and/or species requires more detailed approaches – integrating, for example, life history dynamics as in Bradshaw et al. [13] – we suggest that a general and lower-dimensional framework may be useful for extracting first-order energetic constraints that both shape and potentially limit the general nature of mammalian communities.

That extinction risk appears to increase with body size [61] is integral to our understanding of the Pleistocene extinctions [11–13,53,62] and anthropogenic effects throughout the Holocene [63]. Assessing which energetic walls close in and why, as body size increases, is fundamental for reconciling the nature of extinction [12], particularly when there is size-selectivity [53]. That we observe dynamically-feasible megatrophic interactions to occupy a narrow band of PPMR relationships points to a broader range of interaction structures than are realized in contemporary communities. As the threshold consumer mass decreases with predator specialization, how megafaunal trophic structure changes during extinction cascades may be central for understanding the dynamics of community disassembly [37]. And while these dynamics may arise naturally from the energetic limitations of mammalian interactions, it may be that the added pressures of subsidized harvest, particularly on megafauna, inevitably lead to collapse.

Ethics. Insert ethics text here.

Data Accessibility. Code available on GitHub (ADDRESS)

Authors' Contributions. TR and JDY conceived the study. TR, CK, and JDY designed the model and analyzed the results. TR, CK, and JDY wrote the manuscript.

Competing Interests. The authors have no competing interests

Funding. This project was funded by NSF Award XXX to JDY.

Acknowledgements. We would like to thank Irina Birskis-Barros, Uttam Bhat, Megha Suswaram, and Ritwika VPS for insightful comments and discussions...

Disclaimer. Insert disclaimer text here.

Table 1: Model parameters and values/units

Definition	Parameter	Value/Units
Resource		
density	R	$\mathrm{g/m^2}$
reproduction rate	α	$1/\mathrm{s}$
carrying capacity	k	$\mathrm{g/m^2}$
Consumer		
density	C	$\mathrm{g/m^2}$
body mass	M_C	g
body mass theshold	$M_C^\dagger$	g
theoretical max	$C^{\max}$	$\mathrm{g/m^2}$
timescale of growth from m_1 to m_2	$\tau(m_1, m_2)$	s
reproduction rate	$\lambda_C^{\max}$	$1/\mathrm{s}$
yield coefficient	Y_C	g C/g R
maintenance rate	ρ	$1/\mathrm{s}$
natural mortality rate	μ	$1/\mathrm{s}$
starvation rate	σ	$1/\mathrm{s}$
harvest rate	h	$1/\mathrm{s}$
Predator		
steady state intercept	P_0	8.62×10^{-4} inds/m^2[30]
steady state density	P^*	$P_0 M_P^{-0.88}$ inds/m^2[30]
body mass	M_P	g
body mass theshold	$M_P^\dagger$	g
theoretical max	$P^{\max}$	$\mathrm{g/m^2}$
growth rate	$\lambda_P^{\max}$	$1/\mathrm{s}$
yield coefficient	Y_P	g P/g C
specialization	f	(0,1)
Prop. change starvation rate	χ_s	(-0.99,1)
PPMR intercept	p_0	1.18×10^5 g
PPMR slope	p_1	0.19
Prop. change PPMR intercept	χ_{int}	(-0.99,2)
Prop. change PPMR slope	χ_{slope}	(-0.99,2)
Extinction-inducing harvest rate	$h^\dagger$	$1/\mathrm{s}$
Extinction-inducing harvest pressure	$\psi^\dagger$	inds/yr/A_{CA}
Post-harvest fraction consumer density	ϵ	0.01

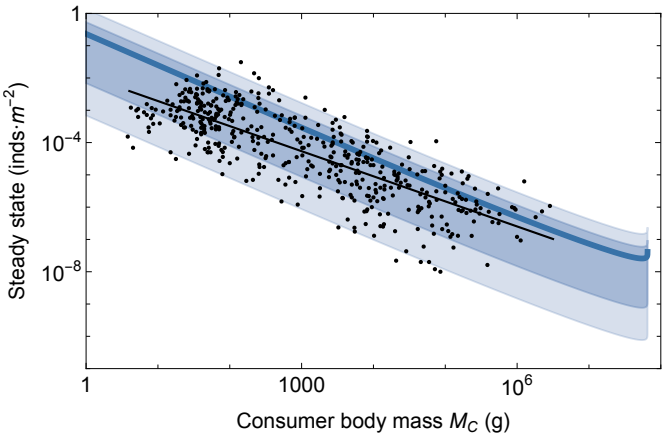

Figure 1: Model predictions of mammalian steady states ($\mathrm{inds} \cdot \mathrm{m}^{-2}$) as a function of herbivore consumer body mass M_C (thick blue line) compared to observational data from Damuth [19] (black points). Variation in steady state densities is capture by allowing the plant resource growth rate to vary as $\alpha = 2.81 \times 10^{-10} : 2.19 \times 10^{-8}\ \mathrm{s}^{-1}$ (dark blue shaded region), and both α and the plant resource carrying capacity to vary as $k = 2.3 : 34\ \mathrm{kg/m}^2$ (light blue shaded region). See Supplementary Appendix XX for details.

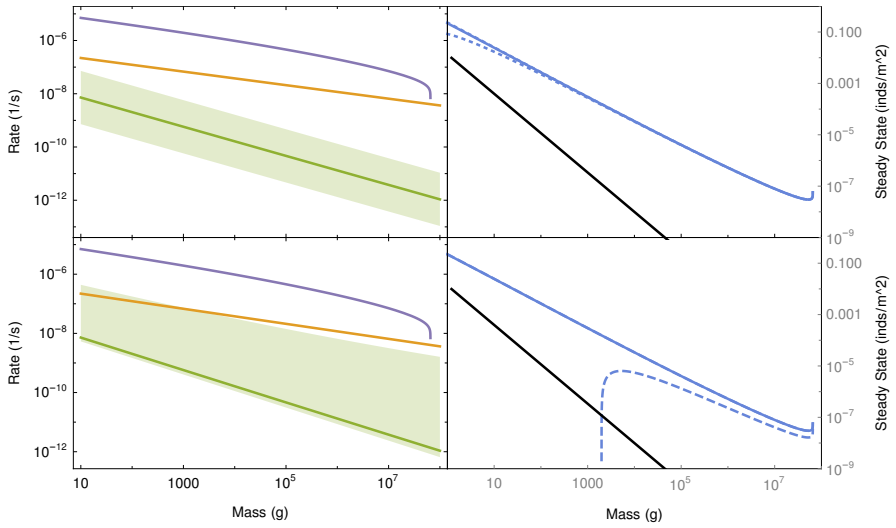

Figure 2: A. The rate of natural mortality μ as a function of consumer body mass M_C (green) relative to the rate of reproduction λ_C (orange) and maximal rate of starvation σ (purple). The range of variation (light green shaded region) is given by allowing the cohort mortality rate q_0 to vary an order of magnitude around its calculated value. B. Population-level effects of increasing the cohort mortality rate q_0 an order of magnitude. C. As in A. but with variation of the actuarial mortality rate q_a by an order of magnitude around its estimated value. D. Population-level effects of increasing the actuarial mortality rate q_a an order of magnitude. The black line denotes the best-fit for the observed mass density relationship [19]; the solid blue line denotes the model prediction; the stippled blue line denotes the model prediction with increased cohort (B) and actuarial (D) mortality rates.

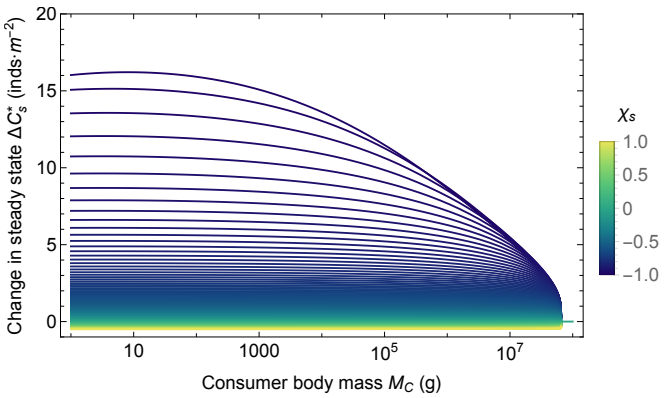

Figure 3: The relative change in consumer steady state ΔC_s^* as a function of consumer body mass M_C given the maximumal rate of starvation $\sigma(1+\chi_s)$ where $\chi_s \in (-0.99, 1)$ (see Eq. 3.1). Declining ΔC_s^* with increasing body mass for lower values of χ_s mean that smaller organisms benefit more from reductions in the rate of starvation.

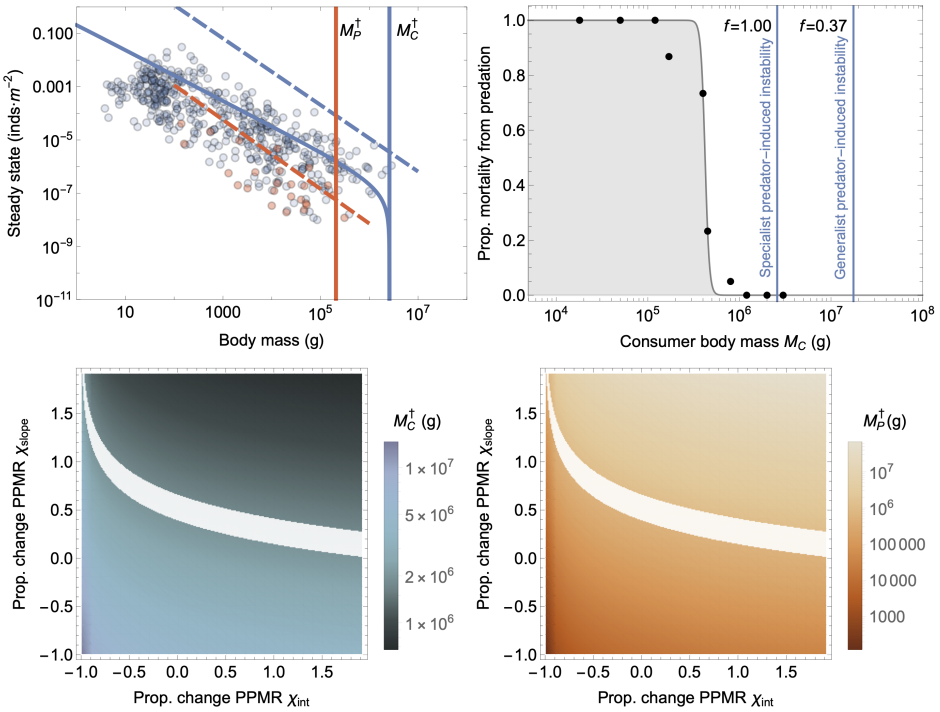

Figure 4: A. Empirical mammalian herbivore (blue points) and predator (red points) mass-densities shown alongside the theoretical maximum herbivore $C^{\max}$ and predator $P^{\max}$ densities as a function of body size. The solid blue curve denotes the predicted herbivore consumer steady state $C^*(M_C)$ with predation mortality. Predicted herbivore $M_C^\dagger$ and predator $M_P^\dagger$ size thresholds (blue and red vertical lines, respectively) reveal where the herbivore consumer population is no longer able to support a predator population. The blue shaded region denotes 'mega' size classes $> 1 \times 10^5$ g. B. Percent mortality from predation for Serengeti herbivores (redrawn from Sinclair et al. [31]) as a function of body mass M_C. Gray shaded region denotes a sigmoidal fit to the data with the inflection at 4.22×10^5 g. Vertical lines show herbivore size threshold under the assumption of predator specialization ($f = 1.00$; $M_C^\dagger = 2.58 \times 10^6$) and generalization ($f = 0.37$; $M_C^\dagger = 1.75 \times 10^7$). C. Threshold herbivore sizes $M_C^\dagger$ across changes to the predator-prey mass ratio (PPMR) intercept and slope (see Eq. 3.4). White shaded region denotes megatrophic threshold sizes, where both $(M_C^\dagger, M_P^\dagger) > 6 \times 10^5$ g. D. As in C., but showing the corresponding threshold carnivore sizes $M_P^\dagger$.

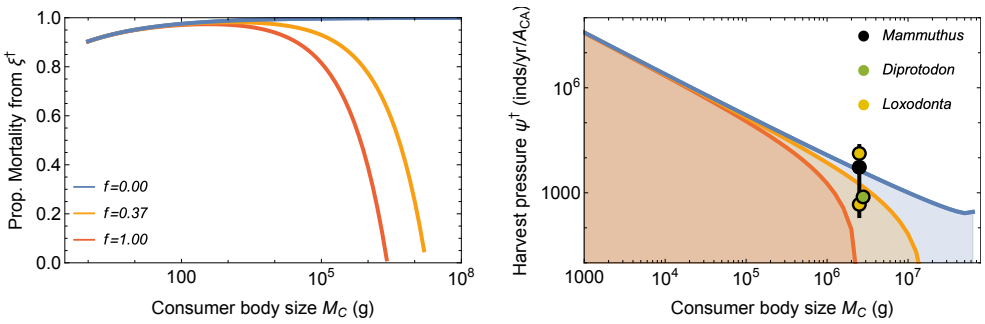

Figure 5: A. Proportion mortality due to an extinction-inducing harvest rate $\xi^\dagger$ without predation ($f = 0$; blue line), with the inclusion of mortality from a generalist predator ($f = 0.37$; orange line), and with the inclusion of mortality from a specialist predator ($f = 1$; red line), as a function of consumer body mass M_C. B. Harvest pressure $\psi^\dagger$ resulting from extinction-inducing harvest (inds/year/A_{CA}) without predation ($f = 0$; blue line), with the inclusion of mortality from a generalist predator ($f = 0.37$; orange line), and with the inclusion of mortality from a specialist predator ($f = 1$; red line), as a function of consumer body mass M_C. Black point and line: median and range of estimated harvest rates for wooly mammoths (*Mammuthus primigenius*) [56]; Green point: estimated harvest pressure for the Australian *Diprotodon* [13]; Lower and upper yellow point: estimated harvest rates for contemporary *Loxodonta* during the early 1800s and just prior to 1987, respectively [57].

References

1. DeAngelis D. 1980 Energy flow, nutrient cycling, and ecosystem resilience. *Ecology* **61**, 764–771.
2. Yodzis P, Innes S. 1992 Body Size and Consumer-Resource Dynamics. *Am. Nat.* **139**, 1151–1175.
3. Hou C, Zuo W, Moses ME, Woodruff WH, Brown JH, West GB. 2008 Energy Uptake and Allocation During Ontogeny. *Science* **322**, 736–739.
4. Lindstedt SL, Schaeffer PJ. 2002 Use of allometry in predicting anatomical and physiological parameters of mammals.. *Lab. Anim.* **36**, 1–19.
5. West GB, Brown JH, Enquist BJ. 2001 A general model for ontogenetic growth. *Nature* **413**, 628–631.
6. Hennemann WW. 1983 Relationship among body mass, metabolic rate and the intrinsic rate of natural increase in mammals. *Oecologia* **56**, 104–108.
7. West GB, Woodruff WH, Brown JH. 2002 Allometric scaling of metabolic rate from molecules and mitochondria to cells and mammals.. *Proc. Natl. Acad. Sci. USA* **99 Suppl 1**, 2473–2478.
8. Kempes CP, Dutkiewicz S, Follows MJ. 2012 Growth, metabolic partitioning, and the size of microorganisms.. *PNAS* **109**, 495–500.
9. Yeakel JD, Kempes CP, Redner S. 2018 Dynamics of starvation and recovery predict extinction risk and both Damuth's law and Cope's rule. *Nature communications* **9**, 1–10.
10. Bhat U, Kempes CP, Yeakel JD. 2020 Scaling the risk landscape drives optimal life-history strategies and the evolution of grazing. *Proceedings of the National Academy of Sciences* **117**, 1580–1586.
11. Alroy J. 2001 A multispecies overkill simulation of the end-Pleistocene megafaunal mass extinction. *Science* **292**, 1893–1896.
12. Brook BW, Sodhi NS, Bradshaw CJ. 2008 Synergies among extinction drivers under global change. *Trends in ecology & evolution* **23**, 453–460.
13. Bradshaw CJ, Johnson CN, Llewelyn J, Weisbecker V, Strona G, Saltré F. 2021 Relative demographic susceptibility does not explain the extinction chronology of Sahul's megafauna. *Elife* **10**, e63870.
14. Murdoch WW, Briggs CJ, Nisbet RM. 2003 *Consumer-resource Dynamics*. Monographs in population biology. Princeton University Press.
15. Calder III WA. 1983 An allometric approach to population cycles of mammals. *J. Theor. Biol.* **100**, 275–282.
16. Robert A, Chantepie S, Pavard S, Sarrazin F, Teplitsky C. 2015 Actuarial senescence can increase the risk of extinction of mammal populations. *Ecological Applications* **25**, 116–124.
17. Alonzo SH. 2002 State-dependent habitat selection games between predators and prey: the importance of behavioural interactions and expected lifetime reproductive success. *Evol. Ecol. Res.* **4**, 759–778.
18. Dunne JA, Maschner H, Betts MW, Huntly N, Russell R, Williams RJ, Wood SA. 2016 The roles and impacts of human hunter-gatherers in North Pacific marine food webs. *Sci. Rep.* **6**, 1–9.
19. Damuth J. 1987 Interspecific allometry of population density in mammals and other animals: the independence of body mass and population energy-use. *Biol. J. Linn. Soc.* **31**, 193–246.
20. DeLong JP, Vasseur DA. 2012 Size-density scaling in protists and the links between consumer–resource interaction parameters. *J. Anim. Ecol.* **81**, 1193–1201.
21. Savage VM, Gillooly JF, Brown JH, West GB, Charnov EL. 2004 Effects of Body Size and Temperature on Population Growth. *http://dx.doi.org.proxy.lib.sfu.ca/10.1086/679735* **163**, 429–441.
22. Smith F, Boyer A, Brown J, Costa D. 2010 The Evolution of Maximum Body Size of Terrestrial Mammals. *Science*.
23. DeLong JP, Okie JG, Moses ME, Sibly RM, Brown JH. 2010 Shifts in metabolic scaling, production, and efficiency across major evolutionary transitions of life.. *PNAS* **107**, 12941–12945.
24. Jones OR, Gaillard JM, Tuljapurkar S, Alho JS, Armitage KB, Becker PH, Bize P, Brommer J, Charmantier A, Charpentier M et al.. 2008 Senescence rates are determined by ranking on the fast–slow life-history continuum. *Ecology letters* **11**, 664–673.

25. Millar J, Hickling G. 1990 Fasting Endurance and the Evolution of Mammalian Body Size. *Funct. Ecol.* **4**, 5–12.
26. Yeakel JD, Bhat U, Newsome SD. 2020 Caching in or falling back at the Sevilleta: the effects of body size and seasonal uncertainty on desert rodent foraging. *The American Naturalist* **196**, 241–256.
27. Schubert KA, Boerema AS, Vaanholt LM, de Boer SF, Strijkstra AM, Daan S. 2010 Daily torpor in mice: high foraging costs trigger energy-saving hypothermia. *Biology letters* **6**, 132–135.
28. Geiser F. 1998 Evolution of daily torpor and hibernation in birds and mammals: importance of body size. *Clinical and experimental pharmacology and physiology* **25**, 736–740.
29. Smith C, Reichman O. 1984 The evolution of food caching by birds and mammals. *Annual Review of Ecology and Systematics* **15**, 329–351.
30. Carbone C, Gittleman JL. 2002 A common rule for the scaling of carnivore density. *Science* **295**, 2273–2276.
31. Sinclair ARE, Mduma S, Brashares JS. 2003 Patterns of predation in a diverse predator–prey system. *Nature* **425**, 288–290.
32. Brose U, Cushing L, Berlow EL, Jonsson T. 2005 Body sizes of consumers and their resources. *Ecology*.
33. Hatton IA, McCann KS, Fryxell JM, Davies TJ, Smerlak M, Sinclair ARE, Loreau M. 2015 The predator-prey power law: Biomass scaling across terrestrial and aquatic biomes.. *Science* **349**, aac6284–aac6284.
34. Barnes C, Maxwell D, Reuman DC, Jennings S. 2010 Global patterns in predator–prey size relationships reveal size dependency of trophic transfer efficiency. *Ecology* **91**, 222–232.
35. Rohr RP, Scherer H, Kehrli P, Mazza C, Bersier LF. 2010 Modeling food webs: Exploring unexplained structure using latent traits. *Am. Nat.* **176**, 170–177.
36. Riede JO, Brose U, Ebenman B, Jacob U, Thompson R, Townsend CR, Jonsson T. 2011 Stepping in Elton's footprints: a general scaling model for body masses and trophic levels across ecosystems. *Ecology letters* **14**, 169–178.
37. Yeakel JD, Pires MM, Rudolf L, Dominy NJ, Koch PL, Guimarães Jr PR, Gross T. 2014 Collapse of an ecological network in Ancient Egypt. *Proceedings of the National Academy of Sciences* **111**, 14472–14477.
38. Pires MM, Koch PL, Fariña RA, de Aguiar MA, dos Reis SF, Guimarães Jr PR. 2015 Pleistocene megafaunal interaction networks became more vulnerable after human arrival. *Proceedings of the Royal Society B: Biological Sciences* **282**, 20151367.
39. Nakazawa T. 2017 Individual interaction data are required in community ecology: a conceptual review of the predator–prey mass ratio and more. *Ecological Research* **32**, 5–12.
40. Kerley GIH. 2005 Prey preferences of the lion (Panthera leo). *J. Zoology* **267**, 309.
41. Hayward M. 2006 Prey preferences of the spotted hyaena (Crocuta crocuta) and degree of dietary overlap with the lion (Panthera leo). *J. Zoology* **270**, 606–614.
42. Hayward MW, Kerley G. 2008 Prey preferences and dietary overlap amongst Africa's large predators. *S. African J. Wild. Res.* **38**, 93–108.
43. Cruz LR, Muylaert RL, Galetti M, Pires MM. 2022 The geography of diet variation in Neotropical Carnivora. *Mammal Review* **52**, 112–128.
44. Cruz LR, Pires MM. 2022 Body mass ratios determine dietary patterns and help predicting predator–prey interactions of Neotropical Carnivora. *Mammal Research*.
45. Burness GP, Diamond J, Flannery T. 2001 Dinosaurs, dragons, and dwarfs: the evolution of maximal body size. *Proceedings of the National Academy of Sciences* **98**, 14518–14523.
46. Sorkin B. 2008 A biomechanical constraint on body mass in terrestrial mammalian predators. *Lethaia* **41**, 333–347.
47. Carbone C, Teacher A, Rowcliffe JM. 2007 The Costs of Carnivory. *PLoS Biol* **5**, e22.
48. van Valkenburgh B, Wang X, Damuth J. 2004 Cope's rule, hypercarnivory, and extinction in North American canids. *Science* **306**, 101.
49. Brook BW, Bowman DMJS. 2005 One equation fits overkill: why allometry underpins both prehistoric and modern body size-biased extinctions. *Population Ecology* **47**, 137–141.

50. Churchill SE. 1993 Weapon technology, prey size selection, and hunting methods in modern hunter-gatherers: implications for hunting in the Palaeolithic and Mesolithic. *Archeological Papers of the American Anthropological Association* **4**, 11–24.
51. Ugan A. 2005 Does size matter? Body size, mass collecting, and their implications for understanding prehistoric foraging behavior. *American Antiquity* **70**, 75–89.
52. Prates L, Rivero D, Perez SI. 2022 Changes in Projectile design and size of prey reveals the role of Fishtail points in megafauna hunting in South America. .
53. Smith FA, Elliott Smith RE, Lyons SK, Payne JL. 2018 Body size downgrading of mammals over the late Quaternary.. *Science* **360**, 310–313.
54. Sethi SA, Branch TA, Watson R. 2010 Global fishery development patterns are driven by profit but not trophic level. *Proceedings of the National Academy of Sciences* **107**, 12163–12167.
55. Jennings S, Blanchard JL. 2004 Fish abundance with no fishing: predictions based on macroecological theory. *Journal of Animal Ecology* pp. 632–642.
56. Fordham DA, Brown SC, Akçakaya HR, Brook BW, Haythorne S, Manica A, Shoemaker KT, Austin JJ, Blonder B, Pilowsky J et al.. 2022 Process-explicit models reveal pathway to extinction for woolly mammoth using pattern-oriented validation. *Ecology letters* **25**, 125–137.
57. Milner-Gulland E, Beddington J. 1993 The exploitation of elephants for the ivory trade: an historical perspective. *Proceedings of the Royal Society of London. Series B: Biological Sciences* **252**, 29–37.
58. Horton DR, Wright RV. 1981 Cuts on Lancefield bones: carnivorous Thylacoleo, not humans, the cause. *Archaeology in Oceania* **16**, 73–80.
59. Wroe S, Myers T, Wells R, Gillespie A. 1999 Estimating the weight of the Pleistocene marsupial lion, Thylacoleo carnifex (Thylacoleonidae: Marsupialia): implications for the ecomorphology of a marsupial super-predator and hypotheses of impoverishment of Australian marsupial carnivore faunas. *Australian Journal of Zoology* **47**, 489–498.
60. Webb S. 2009 Late Quaternary distribution and biogeography of the southern Lake Eyre basin (SLEB) megafauna, South Australia. *Boreas* **38**, 25–38.
61. Cardillo M, Mace GM, Jones KE, Bielby J, Bininda-Emonds ORP, Sechrest W, Orme CDL, Purvis A. 2005 Multiple causes of high extinction risk in large mammal species. *Science* **309**, 1239–1241.
62. Johnson CN. 2002 Determinants of loss of mammal species during the Late Quaternary 'megafauna' extinctions: life history and ecology, but not body size. *Proceedings of the Royal Society of London. Series B: Biological Sciences* **269**, 2221–2227.
63. Estes JA, Terborgh J, Brashares JS, Power ME, Berger J, Bond WJ, Carpenter SR, Essington TE, Holt RD, Jackson JBC, Marquis RJ, Oksanen L, Oksanen T, Paine RT, Pikitch EK, Ripple WJ, Sandin SA, Scheffer M, Schoener TW, Shurin JB, Sinclair ARE, Soulé ME, Virtanen R, Wardle DA. 2011 Trophic downgrading of planet Earth. *Science* **333**, 301–306.